



Swansea University
Prifysgol Abertawe



Cronfa - Swansea University Open Access Repository

This is an author produced version of a paper published in :
Composites Part A: Applied Science and Manufacturing

Cronfa URL for this paper:

<http://cronfa.swan.ac.uk/Record/cronfa29485>

Paper:

Woods, B., Hill, I. & Friswell, M. (2016). Ultra-efficient wound composite truss structures. *Composites Part A: Applied Science and Manufacturing*, 90, 111-124.

<http://dx.doi.org/10.1016/j.compositesa.2016.06.022>

This article is brought to you by Swansea University. Any person downloading material is agreeing to abide by the terms of the repository licence. Authors are personally responsible for adhering to publisher restrictions or conditions. When uploading content they are required to comply with their publisher agreement and the SHERPA RoMEO database to judge whether or not it is copyright safe to add this version of the paper to this repository.

<http://www.swansea.ac.uk/iss/researchsupport/cronfa-support/>

Accepted Manuscript

Ultra-efficient wound composite truss structures

Benjamin K.S. Woods, Ioan Hill, Michael I. Friswell

PII: S1359-835X(16)30211-1

DOI: <http://dx.doi.org/10.1016/j.compositesa.2016.06.022>

Reference: JCOMA 4348

To appear in: *Composites: Part A*

Received Date: 3 March 2016

Revised Date: 10 June 2016

Accepted Date: 28 June 2016



Please cite this article as: Woods, B.K.S., Hill, I., Friswell, M.I., Ultra-efficient wound composite truss structures, *Composites: Part A* (2016), doi: <http://dx.doi.org/10.1016/j.compositesa.2016.06.022>

This is a PDF file of an unedited manuscript that has been accepted for publication. As a service to our customers we are providing this early version of the manuscript. The manuscript will undergo copyediting, typesetting, and review of the resulting proof before it is published in its final form. Please note that during the production process errors may be discovered which could affect the content, and all legal disclaimers that apply to the journal pertain.

Ultra-efficient wound composite truss structures

Benjamin K.S. Woods^{a,*}, Ioan Hill^b and Michael I. Friswell^b

^a *Department of Aerospace Engineering, University of Bristol, Bristol UK, BS8 1TR*

^b *College of Engineering, Swansea University, Swansea, UK SA1 8EN*

Abstract

This paper presents the design, analysis, manufacturing, experimental testing, and multiobjective optimization of a new family of ultra-efficient composite truss structures. The continuously wound truss concept introduced here is a versatile, low cost and scalable method of manufacturing truss structures based on a simple winding process. A prototype truss configuration is shown and experimentally characterized under torsion and three point bending loads. A large deformation implementation of the direct stiffness method is shown to provide good prediction of the stiffness properties of the prototype truss. This model is extended to include strength prediction with multiple failure modes. The design space achievable with these truss structures is then explored through multiobjective optimization using the NSGA II genetic algorithm. These continuously wound truss structures have the potential to provide between one and two orders of magnitude increase in structural efficiency compared to existing carbon fiber composite tubes.

Keywords: Filament winding, Numerical analysis, Mechanical testing, Mechanical properties

Background

There is an ever present need in structural design to minimize mass and maximize structural efficiency. This is true in nearly all engineering disciplines, but is especially true in transportation related applications such as the aerospace and automotive industries where any mass associated with a structure brings recurring costs from the need to transport that weight. There are other factors which also motivate weight reduction more generally, including the

*Corresponding author: ben.k.s.woods@bristol.ac.uk

potential to reduce material and fabrication costs, dynamic and vibration concerns and increased stresses due to self-loading.

Truss structures and space frames have long been preferred solutions to the problem of maximizing structural efficiency, as they allow for very large increases in the flexural rigidity and load carrying capacity achievable from a given amount of material. The primary advantage of a truss over a monolithic or tubular structure is that grouping the material available into discrete local beam members allows for the overall size of a structure built from a given amount of material to be increased to take advantage of the highly non-linear scaling laws governing bending stiffness and strength (as determined by equivalent flexural rigidity) without being overly restricted by the strength limitations inherent in trying to make large, thin walled tubular structures. Another key advantage of truss structures is that they divide the large structure into a number of local members which due to their slenderness, straightness, and attachment methods are able to act in a manner which approaches an ideal two-force member. A two-force member, unlike a beam, experiences only tensile and compressive forces. Structures are considerably stiffer and stronger under axial loading than they are under bending loading, and so the use of trusses allows the material to experience lower stress levels and to be used more efficiently. It is important to note that this only applies if the truss members are straight, as curvature in an element leads to intrinsic coupling of axial and bending loads.

The usefulness of trusses was realized as early as the Ancient Greeks and Romans who used timber frame trusses to support roofs of previously unspanable length,[1,2] and to this day the truss and its three dimensional extension the space frame form the basis of a wide range of structures including bridges, towers, building roofs, light aircraft fuselages, and high performance automobile frames. Truss structures and space frames have been created at nearly all size scales, from the micrometer[3] scale all the way up to the 400 m long Ikitsuki truss bridge in Japan (the world's longest) and the world's largest indoor theme park, Ferrari World, who's elegant space frame structure encloses an incredible 86,000 m².

One of the primary drawbacks of existing truss structures is the difficulty and expense of manufacturing them from separate individual members, often numbering in the dozens, hundreds, or even thousands which must be individually attached together at a series of nodes. This requires first the fabrication of the truss members, which are often different sizes and lengths and then attaching them with a large number of bolted or welded joints. Additional gusset plates are often required to strengthen these joints, further adding to the part count and labor requirements. While the structural advantages of trusses outweigh these added manufacturing costs for many larger structures,

there appears to be a real world lower limit on the size of truss structures. It is relatively uncommon to see built up truss structures with individual member lengths smaller than roughly 10 cm or overall structural lengths less than a few meters. Since the strength and stiffness advantages of trusses exist at all engineering length scales, it must be the case that the reason for this practical lower limit is not physical but economical. In this size region, traditional built up truss structures are more difficult and therefore more expensive to make (due to the small size of individual members). On the other hand, it is exactly in this size range that tubular and monolithic structural members (extruded metal profiles for example) are most often made and so they benefit from massive economies of scale in their production. This gap in the implementation of truss structures unfortunately exists exactly in the size range of our most common daily interactions with our engineered world, which results in many of the structures which we encounter in our day-to-day lives which would benefit from the structural efficiency of trusses do not employ them; with furniture being one relevant example.

Several research groups have investigated ways of manufacturing composite truss structures at this “missing” length scale. Shütze presented the development and implementation of composite truss beams of equilateral triangle cross section which were manufactured using traditional methods of attaching individual members together with bonded joints and reinforcing gusset plates.[4] These truss beams were designed for use within the structural frame of a rigid airship. Weaver and Jensen introduced a complex truss beam structure manufactured with a braiding machine.[5] This concept is known as the IsoTruss® and is currently under commercial development. The IsoTruss® concept has the advantage of being made from continuous elements and therefore not requiring the manufacture of separate individual members which are then connected together. Instead, as seen in Figure 2, a braiding machine is used in conjunction with a multi-point node supporting apparatus to allow for the individual members to be created by winding various tow elements together. The geometry of these truss structures is complex, with eight to twelve nodes around the perimeter of the truss forming a star shaped, non-continuous cross section with the fiber running in straight segments between nodes. This creates a fully three dimensional structure of overlapped and interlaced tetrahedron elements. In the process shown in Figure 2, there is no mandrel around which the truss is braided, which therefore requires the use of individual hook type supports for every single node. These supports must be able to translate along the length of the truss as it is wound, and must remain there until the polymer matrix bonding the tows together is fully cured. Other work by the same research group and others has used internal mandrels to make the same basic structure,[6–8] and have considered winding based methodologies

instead of braiding, but in this case the non-continuous cross section, visible in Figure 2, and the need to support the material at each node creates captive mandrel geometries, which requires the use of complex multi-component mandrel solutions that can be disassembled, collapsed, or dissolved for removal after the composite has cured. Other researchers have considered modified forms of braided truss structures that greatly simplify the geometry, but they do so using a circular cross section mandrel which creates curved segments.[9] These curved sections are inherently less stiff and weaker than straight elements between nodes because they will act as beams under combined axial and bending loading instead of as two-force members. While these various types of braided truss structures have made a considerable advance towards the realization of smaller scale truss structures that can be integrated into any number of applications, they suffer from the requirement of needing braiding machines, which are mechanically complex apparatuses requiring significant capital investment. They also suffer from complex or compromised truss geometries which will invariably affect their performance and cost.

Filament winding has been used to create a class of lattice structures known as anisogrid composite lattices, with a large body of work undertaken in Russia going back to the 1980's.[10,11] These structures are made by stacking up successive windings of wetted out tow to form a lattice network of rib structures around the circumference of a cylindrical or conical shell. Due to the large number of overlapping tow segments which stack up at the node locations and the fixed overall height of the rib, this approach requires fairly low fibre volume fractions, on the order of 35%.[11] This low volume fraction provides physical space for the tows to be co-located at the nodes without increasing the overall height, with the volume fraction at the node then being double that seen elsewhere. In theory the volume fraction could be as high as 50% and still allow for this effect, but the specific strength of these structures levels off after 35% volume fraction. In order to effectively align, and consolidate the stacks of tow which make up each rib member, foam or elastomeric moulds are placed around the mandrel which have grooves to contain the windings. Producing these complex moulds (which in the case of foam are sacrificial) adds significantly to the complexity of the underlying filament winding process. Prototype structures have shown excellent mechanical properties, with weight savings over aluminium equivalents of 30-40%, but the complexity of the process and limited fibre volume fraction complicates widespread adoption.

There is a related body of work into the development of sandwich core structures manufactured from composite lattice structures.[12-14] While these three dimensional, planar structures have a different intended use than the

beam like structures investigated here, and use significantly different manufacturing methods, this work has shown significant improvement in the structural efficiency of sandwich structures.

To address the underlying economics of truss manufacturing in general, what is needed is a construction method that reduces the manufacturing complexity by eliminating the process of fabricating individual members to be assembled in a piece by piece fashion. Ideally such a process would be continuous, scalable, and use low cost materials and equipment. Furthermore, if this process used fiber based composite materials, then it would gain further advantage from the excellent mechanical properties of these materials. To improve on the performance and economics of the continuous truss structures developed in previous literature, what is needed is a simpler concept using lower cost processes which retains the properties of true truss structures (straight members for example). To this end we introduce the continuously wound composite truss structures under development here.

Continuous Wound Truss Concept

In order to allow for the creation of a new class of structural solutions with excellent structural efficiency stemming from low mass and high stiffness and strength, a novel continuous winding process has been developed which allows for the creation of truss structures from composite materials at low cost and with high production rates. This winding process is an adaptation of existing filament winding technology. In existing technology, resin impregnated tows of fiber are wound over an underlying mandrel to create a continuous tubular structure. The tow is wrapped under tension so that it flattens out and allows for the gradual building up of thickness of material with minimal gaps in between adjacent tows. This process is typically used to produce round cross sections, but is adaptable to a wide range of cross-sectional shapes. To date, filament winding has been primarily limited to tubular and closed pressure vessel type structures.

To instead create non-continuous, open truss type structures with discrete, individual members, the filament winding process is adapted in several key ways. Figure 3 shows a schematic overview of this process. Firstly, the winding mandrels used are not curved in cross-section but instead are polygonal, with for example a triangular shape. At the vertices of the polygons, accommodations are made to support pre-made longitudinal members which will bond to the wound fiber members to form the chord members of the truss. These chord members may be made from a range of materials and manufacturing processes, with carbon fiber reinforced polymer matrix pultrusions

being a relevant example. The straight sides of the mandrel allow the wound fiber members to also be straight in between the chord members, which significantly increases their strength and stiffness. During winding, the feed stock material for the wound fiber members will bridge between the chord members at a pre-set angle to them, wrapping around them to form bonded nodes but stretching unsupported between them to create the individual members of the shear web. The final major adaptation of the winding process is in the form of the feed stock material wound around the mandrel. With these truss structures each winding of this feed stock is intended to create the discrete wound shear web members in their entirety. Therefore the amount and arrangement of the material in this feed stock will be significantly different from traditional filament winding. For example, instead of a flat tow of unidirectional carbon fibers, the feed stock for a wound truss might instead be braided from a number of individual tows to create a larger cross-sectional area, a round instead of flat profile, and off-axis fiber content to improve robustness and damage tolerance. While there are indeed a very wide range of methods for controlling the shape and properties of the wound members, many of which are discussed in Woods, Berry and Stavnychiy,[15] the underlying differentiating principle is that a single wrap of this feed stock between two adjacent chord members is intended to create a complete local member that will behave in a manner analogous to the different discrete members of a truss or space frame. From the perspective of the built up truss structure, the winding operation creates the shear web between the chord members using a single strand of feed stock wound around the chord members, with the discretely assembled joints of typical truss structures replaced by bonded joints which are automatically formed during the winding process. The resulting increase in structural efficiency achievable with this modest modification to the process is very significant, as will be shown. Essentially, the material that usually forms a thin, continuous tube wall in traditional filament winding is being bunched together to create non-continuous, discrete members of a much larger relative thickness. Crucially, this localization of material and resulting increase in thickness allows the truss to take advantage of the highly non-linear relationship between the thickness of a structural member and its strength under bending and compression loadings. This in turn allows for the creation of a larger structural cross-section for a given weight and applied loading, resulting in non-linear increases in the achievable flexural rigidity and stiffness properties.

It can be seen that this process has several distinct differences from the IsoTruss® described above. The geometry of the finished truss is considerably simpler, which significantly impacts the difficulty of manufacture. Note the simplicity of the winding mandrel needed here, which is prismatic and can therefore be constructed simply

from any number of materials and methods. Being prismatic, the mandrel is also not mechanically captive within the truss geometry. After the truss has cured, it is possible to simply and quickly slide it off of the mandrel. On the other hand, the hanging nodes of the IsoTruss® seen in Figure 2 require support during cure that must come in the form of external hook type supports or from an internal mandrel. This mandrel however, will be captive and unable to be removed from the part unless it is destroyed (as with a sacrificial mandrel) or unless it is collapsible or can be disassembled to move the node supports out of the way of the structure. Such a mandrel is of course feasible (as is shown in [7]), but it is clear that the approach taken here is significantly simpler, and is therefore likely to be considerably lower cost and more flexible. Another primary advantage of the current method is the simplicity with which commercially available tubes can be adopted for the longitudinal members, which has several advantages. The low cost of existing composite manufacturing techniques (such as pultrusion and pullwinding) can be taken advantage of, and it is significantly easier to make the longitudinal elements tubular instead of solid, which has significant benefit for their local bending stiffness and buckling strength.

First conceived in 2009, the continuously wound truss concept was introduced as a way to improve the performance of blade spars for a human powered helicopter then under development at the University of Maryland. The initial application of the concept was in the 6.5 m long primary spar structures for the eight blades of the quad-rotor Gamera human powered helicopter. The cross-section of these spars was based on a triangle with a center-to-center distance between chord (longitudinal) members of 89 mm. The completed spars weighed 1.4 kilograms and were able to support a bending moment of over 325 Nm. The technology was first flown on May 12th, 2011 in what was the third ever human powered helicopter to take flight. The design of this helicopter, including its wound truss spars is discussed in Berry *et al.*[16] Following this success, a number of different scaled down versions of the wound truss architecture were used to build nearly every structural component on a revised Gamera II design, shown in Figure 4. The adoption of the wound truss technology led directly to a 35% reduction in vehicle weight, allowing Gamera II to break a series of FAI official world records in human powered flight. A US Patent on the technology is currently pending.[15] Gamera also adopted a multi-scale truss design in its airframe, wherein the overall airframe structure connecting the four rotors to the cockpit was a truss and also the individual members of that truss were themselves trusses, which were wound in the manner described here. This approach provided very high levels of structural efficiency and is applicable to a number of other applications.

Analysis of Wound Composite Truss Structures

A useful level of initial insight into the performance and design limitations of these truss structures can be gained through simple numerical modeling of their behavior. The direct stiffness method (DSM) provides a robust approach to the analysis of truss structures. It is employed here with the individual members of the wound truss being modeled as truss members with the standard two-force member assumption.[17] A parametrically driven, three-dimensional, nonlinear (large deflection) implementation of the DSM was coded in Matlab for this work, allowing for truss geometries and material properties to be easily changed and for the response of the truss (forces, displacements, stresses) under a variety of loading conditions to be quickly analyzed. The DSM analysis was extended to include strength and stability limits for the truss members based on material failure stress properties and the Euler column buckling model applied locally to each individual member of the truss. The stiffness predictions of the DSM model under bending and torsional loading will be validated against experimental results for a prototype truss, and the boundary condition assumptions underlying the Euler buckling model will be benchmarked against experiment.

The direct stiffness method is a standard matrix based solution method to find the force and displacement behavior of mechanical structures and it is used extensively in a wide range of academic and commercial finite element analysis programs. It is implemented here with the two-force member assumption commonly employed for truss and space frame analysis, which results in significant reduction in the number of degrees of freedom and associated computational cost. The DSM analysis used here is essentially the same as what would be found in a commercial Finite Element Analysis (FEA) code employing beam elements and freely rotating nodes. In such cases, commercial FEA codes will typically also solve very quickly. The major advantage of directly coding the DSM into Matlab is that it allows for the entire process of geometry definition, connectivity matrix definition, displacement solution, and strength checks to be automated within a single piece of software, greatly simplifying and reducing the cost of large multi-objective optimization studies.

As this approach is generally well known,[17,18] its implementation here will not be discussed at length, instead a brief overview of the method is given with attention paid to the three dimensional implementation used here, and the modification applied to allow for large deflections.

The structural equations are formulated along the lines of the approach laid out in Kardestuncer, as it provides a particularly compact form.[17] We start by considering a single member in three dimensions formed between nodes

i and j , as shown in Figure 5. The local coordinate system is defined as a single vector x along the length of the member ij .

Directional cosines for the two end nodes are found from the global frame coordinates of the two end nodes:

$$l_i = \frac{X_i - X_j}{L_{ij}} \quad m_i = \frac{Y_i - Y_j}{L_{ij}} \quad n_i = \frac{Z_i - Z_j}{L_{ij}} \quad (1)$$

$$l_j = \frac{X_j - X_i}{L_{ij}} \quad m_j = \frac{Y_j - Y_i}{L_{ij}} \quad n_j = \frac{Z_j - Z_i}{L_{ij}} \quad (2)$$

Where $[X_i, Y_i, Z_i]$ are the coordinates of node i in the global coordinate frame and similarly for j . After deformation and displacement of the member to a new position defined by the nodes i' and j' , the axial deflection of the member along the local axis at each node (δ_i and δ_j respectively) can then be found from changes to the global node coordinates ($\Delta_x, \Delta_y, \Delta_z$) using the rotation vector R_{ij} .

$$\delta_i = R_{ij} \Delta_i, \quad \delta_i = [l \quad m \quad n]_i \begin{bmatrix} \Delta_x \\ \Delta_y \\ \Delta_z \end{bmatrix}_i, \quad \delta_j = [l \quad m \quad n]_j \begin{bmatrix} \Delta_x \\ \Delta_y \\ \Delta_z \end{bmatrix}_j \quad (3)$$

The force in each member (in the local frame) is then found

$$f_{ij} = \left(\frac{EA}{L}\right)_{ij} \delta_i - \left(\frac{EA}{L}\right)_{ij} \delta_j = \left(\frac{EA}{L}\right)_{ij} R_{ij} \Delta_i - \left(\frac{EA}{L}\right)_{ij} R_{ij} \Delta_j \quad (4)$$

And then transformed into the global frame by pre-multiplying by the transpose of the rotation vector

$$F_{ij} = R_{ij}^T \left(\frac{EA}{L}\right)_{ij} R_{ij} \Delta_i - R_{ij}^T \left(\frac{EA}{L}\right)_{ij} R_{ij} \Delta_j \quad (5)$$

$$F_{ij} = \left(\frac{EA}{L}\right)_{ij} R_{ij}^* (\Delta_i - \Delta_j) = k_{ij}^* (\Delta_i - \Delta_j) \quad (6)$$

$$R_{ij}^* = R_{ij}^T R_{ij} \quad (7)$$

The global stiffness matrix K is then assembled from the member stiffnesses, k_{ij} (which are in global coordinates) for the N different members in the truss structure with consideration of the connectivity between the members.

$$K = \sum_{i=1}^N k_{ij} \quad (8)$$

In this work, the connectivity between members is hard coded for a single unit cell of the repeating truss geometry, with successive unit cells using this same basic connectivity but with the member indexes offset to reflect its position in the truss. Once the global stiffness matrix is assembled, boundary conditions and known node forces (the applied loads in this case) are applied by substituting them into the appropriate entries in the global force equation.

$$F = K\Delta \quad (9)$$

The global force equation is then solved, thereby providing the forces in each member and the displacement of all nodes. This method is readily adaptable to a parameter driven definition of the wound truss structures, allowing for analysis of a wide range of geometries and material properties. It is also computationally very inexpensive, allowing for large batch analysis and optimization. One limitation of this implementation is that it is reliant on the assumption that the node deflections Δ are small enough to not alter the overall shape of the truss. The high aspect ratio trusses explored here are likely to undergo large global displacements, even with small local member deformations, and so this assumption is not likely to be valid. A modification to this analysis method is therefore needed to allow for large truss displacements.

It is worthwhile to note at this point the simplified manner in which this analysis method considers the nodes of the truss. In reality, the locations at which the wound shear web contacts itself and the chord members are geometrically complex, with each node having two layers of winding stacked on top of each other. Furthermore, each filament travels a quasi-helical path around the longitudinal member, and bonded joints are created of complex shape and size dependent on a number of processing variables are formed. This arrangement is likely to introduce a number of non-linear effects and is likely to influence the strength of the node. The stiffness and strength properties of the nodes are expected to be important to the performance of the overall truss structures, particularly their ultimate strength, but as the DSM considers the node as a single point in space where all of the bonded elements exist, it is too low fidelity to capture any of the details of the node mechanics. We will continue with the DSM for the time being, as it is a very useful initial design tool, but it is likely that future development of the concept will require significantly better understanding of the behaviour of the bonded nodes.

Large Displacement Formulation

In order to allow for large displacement (but low strain), non-linear deflections of the truss structures, an incremental loading approach is combined with a geometry updating scheme.[19] The full design load was applied incrementally in small steps, with the truss geometry updated between each step by setting the deformed shape from the previous load increment to be the starting shape of the current increment. The forces in each member induced by the previous load step are also used as the starting forces for the current load increment, with the additional increment of the applied load superimposed. The solution is iterated until the full load has been applied.

Increasing the number of load increments used increases the ability of the analysis to capture large deformations but it also has a significant impact on the solution time, and so a tradeoff between solution accuracy and computational cost exists. However, as is true in many numerical methods there exists diminishing returns in accuracy improvement, and so a convergence study was performed to determine the number of load increments required for an acceptable level of accuracy with minimized cost. An example of the convergence behavior of this analysis can be seen in Figure 6, where the predicted rotation of a truss under torsional loading is shown for three different applied torque levels and for a range of loading steps from 1 to 100. The twist angles have been normalized to the converged twist result to allow for more direct comparison of the convergence behavior between the different load levels. It can be seen that increasing the load applied leads to more loading steps being required to accurately capture the response. This is a result of the non-linearity of the large deflections involved. Even for very large applied torques (indeed, 15 Nm is beyond the failure load for this particular truss) 50 load steps is more than sufficient, as the estimated twist at this point is less than 0.1% different from the final converged prediction. For all of the analysis presented below, 50 loading steps are used.

Example Results of DSM Analysis

To show the ability of this analysis to capture large deflections under a variety of loading conditions, some representative results from the DSM truss analysis are shown in Figure 7. These include a cantilevered truss under tip load, three point bending loading, and torsional loading. Note that for the cantilevered and three point bending examples the force remains vertical, while in the case of torsional loading the three discrete forces which create the net torque on the structure rotate with the deformed geometry during the incremental loading process. The truss configuration shown in these examples is very similar to the manufactured prototype described below.

Experimental Validation of Direct Stiffness Method Analysis

To build confidence in the applicability of the DSM to these wound composite truss structures, two sets of experiments were carried out on prototype trusses manufactured at Swansea University. The first subjected the truss to bending loads using a three point loading apparatus, and the second applied torsional loads using an in-house produced rotational loading rig. Details of the experimental test specimens will first be given, followed by

descriptions of the testing methods, and finally a comparison between the experimentally measured properties and the predictions from the DSM analysis discussed above.

Truss Geometry and Manufacturing

The trusses used for this testing were manufactured on the mandrel and winding apparatus shown schematically in Figure 3. As seen in Figure 8, the three chord members are arranged in an equilateral triangle with a center-to-center distance h of 30 mm, and were taped to the mandrel before winding. They are commercially available carbon fiber pultruded tubes with an outer diameter of 3 mm, inner diameter of 2 mm, and a length of 1 m. Two strands of 12k carbon fiber tow (Hyusong Tansome H2550 A10 fiber) were wetted out with West System epoxy and wound around the mandrel, starting from a fixed point at one end, back and forth six times to create the shear web members on all three sides and in both directions. The node locations were marked on the mandrel at 33 mm spacing and the winding stock was aligned with each successive node by eye as a gear motor rotated the mandrel. This node spacing allows for 30 unit cells over the length of the truss, resulting in an effective length of 990 mm and a shear web angle of $\theta = 47.7^\circ$. Temporary winding posts were placed at the ends of the truss to allow for the direction of winding to be reversed. After the epoxy was cured, the truss was rotated slightly relative to the mandrel allowing it to easily slide off, leaving the mandrel ready for winding another truss. The cured shear web members have a diameter of 1 mm. Manufacturer supplied material properties were used for the pultruded chord members, while tensile testing of shear web specimens showed an elastic modulus of 105 GPa.

Bending Stiffness Testing

Bending stiffness was experimentally measured using a three point bending arrangement. The truss was supported at node locations by steel blocks as seen in Figure 9. The distance between supports was 28 unit cells (924 mm). The load was applied by stacking known masses on a loading tray, which was suspended from the top center node of the truss via a kevlar loading strap. The vertical displacement of the top center node was recorded using a laser displacement sensor rigidly mounted above the truss on a separate beam, with the laser pointing down onto a small metal reflector attached to the truss. Load was added in roughly 1 kg (9.81 N) increments, with each added mass weighed on a precision scale. The test was repeated three times and the results averaged.

Torsional Stiffness Testing:

The torsion loading apparatus is somewhat more involved than the three point bending rig due to the need to properly restrain the fixed end and to apply a pure torsion load with no induced bending. The setup used can be seen in Figure 10. One end of the truss is anchored to a table through a fixed end plate, while the other end is supported in a bearing block that allows freedom of rotation as well as freedom to change in length (to allow foreshortening under rotation). A moment arm was attached to this end of the truss, extending perpendicularly from the truss axis. Masses were hung off this moment arm, 250 mm from the truss axis. The use of a bearing block allows for the vertical load to be reacted directly into the table, leaving the truss to react only the torsion resulting from the force acting at a moment arm. Short sections of threaded rod were bonded into the ends of the truss chord members. These rods extended past the length of the truss, allowing the truss to be secured to the moment arm and fixed end plate using nuts and washers. The moment arm also included provisions for mounting a digital angle sensor for recording the deflection angles.

Torsional Strength Testing:

After completion of stiffness testing, three separate trusses were tested to failure on the torsion rig. All three broke during the same load application step. Having held 0.24 Nm, they all broke during application of 0.255 Nm of torque, indicating a failure strength somewhere between those two values. In all three cases, the failure mode was local buckling of shear web members under compression. The location of failure along the length of the truss varied, although since torque is constant along the truss in this loading condition, it would be expected that failure could occur anywhere. The scope of this initial strength testing is admittedly limited, but it provides a useful benchmarking point for the direct stiffness method, as will be seen. A much more thorough treatment of failure modes in composite truss structures is given in [8]. In this case, the torsional loading was primarily being carried by the shear web, as would be expected, and the portions of the shear web under compression are the likely points of failure initiation as they are prone to buckling. Consideration of these buckling modes is therefore essential in the design process.

Comparison of DSM to Experimental Results

The large displacement DSM analysis code was run for both loading conditions. In Figure 11a the comparison between experiment and analysis for the three point bending tests is shown. The agreement between the two is

fairly good, with the analysis slightly overpredicting the stiffness of the actual truss. The relative root mean squared error between the experiments and analysis is 7.8%. The equivalent flexural rigidity of the truss can be backed out from both the DSM and the experiments using linear least squares regression fitting of the data to find the slope P/w and the Euler Bernoulli beam equation for a simply supported beam of length L .

$$EI_{eq} = \frac{P L^3}{w 48} \quad (10)$$

The DSM predicts an equivalent flexural rigidity, $EI_{eq,DSM} = 184.27 \text{ Nm}^2$, compared to a measured value of $EI_{eq,exp} = 179.05 \text{ Nm}^2$, an error of 2.9%.

A comparison between experiment and analysis for the torsional loading case is shown in Figure 11b. There is a mild non-linear trend in the experimental data, but overall the agreement is again quite good. In this case the relative root mean squared error is 6.4%. In a similar manner to the calculation of equivalent flexural rigidity shown above, equivalent torsional rigidity of the truss can be found according to:

$$GJ_{eq} = \frac{T}{\theta} L \quad (11)$$

For this geometry the DSM predicts a $GJ_{eq,DSM} = 14.96 \text{ Nm}^2$ whereas the experimental data shows $GJ_{eq,exp} = 14.30 \text{ Nm}^2$, a difference of 4.6%. Taken together, these tests show that despite the simple way in which the DSM analysis models these wound truss structures, it is able to capture their stiffness properties with a good degree of accuracy. This level of accuracy is quite useful for initial, low fidelity investigations into the potential benefits of using this manufacturing process.

Comparison to Commercially Available Composite Tubes

One of the primary aims of this study is to show the incredible potential these wound truss structures have, which in part requires comparing them to existing composite structural members. To this end, several commercially available alternatives were modeled as well. While there exists a very wide range of composite structural member geometries, configurations and manufacturing methods available, and even more which could be custom produced for a given application and loading situation, for the sake of comparison we will consider three widely available families of commercial products which best match the use and application set envisaged for the wound trusses; namely pultruded, roll wrapped, and pull wound carbon fiber reinforced polymer tubes.

Pultrusion is a high throughput, low cost manufacturing process for composite tubular and rod sections of constant cross section.[20] In some ways a development of the extrusion process commonly used with polymers

and metals, pultrusion pulls dry fibers (carbon, fiberglass etc.) through a thermoset resin impregnation bath and then through a heated die having the desired cross section of the finished part. This continuous process allows for virtually unlimited part length, high dimensional accuracy, and low recurring part cost, although the initial capital investment required is significant. Pull winding is a further modification of pultrusion which introduces significantly more off-axis fiber content by including a braiding machine before the pultrusion die which braids fiber tow around the axial fiber feedstock at a range of angles.[21] The higher off-axis fiber of pull winding allows manufacture of larger diameter tubes with thinner walls compared to pultruding. Roll wrapping is a non-continuous process wherein plies of composite fabric, most often pre-impregnated with resin, are wrapped around a cylindrical metal mandrel and cured under vacuum pressure.[22] While this process is non-continuous and requires significant hands-on labor, it is highly adaptable and has low capital costs.

For the sake of this initial comparison between existing technologies and the wound truss members, details of a number of tubes of each manufacturing methods were collected from various manufacturers. For many of the tube outer diameters, multiple wall thicknesses were available. In these cases, only the tube with the thinnest wall was included in the comparison, as this will have the best performance with the stiffness metrics explored here. This ensures that the tubes perform as well as possible in this stiffness based comparison.

Estimating Mechanical Properties of Existing Tube Manufacturing Methods

In this paper we will compare the stiffness and mass properties of these families of commercially available tubes to what is potentially achievable with the wound truss technology. In order to estimate the flexural rigidity EI of the different tube sizes manufacturer supplied values are used for flexural elastic modulus, E_f , and geometrically calculated second moments of area for round tubes, I , according to:

$$I = \frac{\pi}{4}(r_o^4 - r_i^4) \quad (12)$$

$$EI = \frac{\pi E_f}{4}(r_o^4 - r_i^4) \quad (13)$$

The linear density (mass per unit length), λ , is found from cross sectional area A and manufacturer supplied material density ρ :

$$\lambda = \rho A = \rho \pi (r_o^2 - r_i^2) \quad (14)$$

It is important to note that the strength properties of the different tubes are not directly compared to the wound trusses in this work. Including meaningful predictions of thin walled tube strength is not trivial, as the tubes are

likely to fail at load levels which are below the theoretical maximum stresses of the material obtained by a simple cross sectional analysis.[23] This is especially true as the ratio of tube diameter to wall thickness increases and effects such as crippling, non-linear deformations, and loading point stress concentrations lead to significant reductions in overall tube strength. Since large diameter, thin walled tubes will provide the best performance in terms of flexural rigidity available from a given linear density, a stiffness based comparison would favor tubes that are likely to have low relative strength. The results of this comparison would be quickly muddled by attempts to analyze the many different failure modes of the different composite tube construction methods considered, and so for the sake of clarity and within the context of this initial investigation, a direct comparison of strength between the tubes and trusses is not undertaken here. The DSM analysis does allow for some initial consideration of stability and strength for the trusses in a straightforward manner, and so as discussed below strength will be considered for the trusses, but not as a direct comparison to the commercial tubes.

Optimization of Truss Structural Geometry

In order to explore the effectiveness of the proposed truss structures across a broad range of sizes and applied loading, a multi-objective optimization of truss geometry was undertaken by wrapping a two-objective Genetic Algorithm (GA) optimization algorithm around the previously validated Direct Stiffness Method analysis. This optimization has two concurrent objectives: to maximize the effective flexural rigidity, EI , of a cantilevered continuously wound truss under tip load while also minimizing the truss mass per unit length, which is referred to herein as linear density, λ . A number of design constraints and checks were applied to ensure that realistic, feasible truss geometries were produced, and the optimization process was repeated for a number of different loading levels, as the applied tip load the truss must react is a primary design driver. The multi-objective implementation of the NSDGA-II optimization algorithm[24] in the Matlab Global Optimization Toolbox was used, which allowed for easy integration of the DSM routine and supplementary failure analysis scripts, which were also written in Matlab. The GA optimization runs used large populations of 3000 individuals and were run for 150 generations, and a Pareto fraction of 0.7 was used to help ensure good coverage of the Pareto frontier and convergence on the optimal solutions. The low computational cost of the DSM model made these large runs tenable on a single consumer Intel i7-3540M (quad core, 3.0 GHz, 16 GB RAM) computer, with an optimization run taking less than 9 hours to

complete the roughly 450,000 large displacement truss evaluations required for each optimization run. The details of the optimization will now be discussed, followed by presentation and discussion of the results.

Truss Geometry Definition

This study was designed to investigate the performance of the wound trusses over a wide range of sizes and weights. The configuration studied used three chord members arranged in an equilateral triangle, as shown in Figure 8. The primary geometric design variables explored in this optimization are shown schematically in Figure 12.

Wide bounds were used for the primary geometry variables (as listed in Table 1), with one important exception, which was truss length. In this study the length of each truss is coupled to its height, with the truss being nominally 20 times longer than the center to center distance between chord members, rounded to the nearest unit cell. For this study the shear web is assumed to be a solid round rod with a diameter between 0.2 mm and 5 mm. While tubular and sandwich structured versions of the shear web have been designed and manufactured (resulting in highly non-linear increases in local buckling strength)[16], for the sake of this analysis a simple rod cross-section made from a continuous bundle of wetted out carbon tow was assumed. The chord members are chosen from commercially available tubes, and so unlike the others this design variable is an integer, with the values 1-34 referring to specific tubes on a compiled list of 34 commercially available pultruded and pull wound tubes with outer diameters from 0.7 mm up to 25 mm. Figure 13 shows the outer diameters and wall thickness to outer diameter ratios of the 34 different tubes considered. Manufacturer supplied material properties corresponding to the different tubes were used as required.

Loading Condition

In this study the trusses were supported and loaded in a cantilevered tip load configuration. The first three nodes (comprising one end of the truss) were prescribed fixed displacements of zero in all three directions and a vertical force was applied to the uppermost node on the opposite end, as shown in Figure 7a. This force remained vertical during deformation and its magnitude was scaled by the mass per meter of the truss. The tip load was defined as:

$$P = k_p \lambda \quad (15)$$

where λ is the linear density (in kg/m) of a given truss being studied and k_p is the loading factor (units of Nm/kg). The value of k_p ranged from 125 to 1000 in this study.

While there are several ways in which the length and load applied to different sizes of truss could be scaled (or indeed not scaled if constant forces/lengths were used), the method used here has several advantages. Firstly, the use of 20 truss segments for the overall length helps to ensure that the truss behaves globally as a beam. This ensures the structures are appropriate for their intended manufacturing method and usage, and that the analysis methods used are valid. The rather good agreement between the DSM and the experimental results shown above is likely due in part to the slenderness of the structure and the small relative size of the individual members. These factors help to create a more ideal two-force member condition. By prescribing the truss length to be 20 times its unit cell length all of the trusses studied will have reasonably high slenderness, helping to build confidence in the use of DSM across such a broad range of shapes and sizes. Additionally, as the underlying intention of this optimization is to study the relationship between truss mass and stiffness (where both have been optimized), the use of a tip load which scales with mass allows for meaningful results over a wide range of linear densities, as it is generally true that larger/heavier structures will have to carry larger loads. This is more useful than fixed load magnitudes (which were also considered but not pursued), as any given fixed load will only be relevant to a narrow range of truss sizes/masses.

Failure Analysis

Strength analysis is included in this optimization to ensure that each candidate truss geometry can withstand the applied load. There are several possible failure modes which are considered, and a failure by any mode in any member of a truss leads to a penalty function being applied to ensure its removal in the next generation of the optimization. Since the trusses are modelled as being composed of two force members, the failure modes considered for each individual member include local buckling, compressive failure, and tensile failure. In all cases, a safety factor of $SF = 1.5$ is applied. The individual member forces are directly available from the output of the DSM, so the failure checks are applied to each truss member (i) as follows:

$$F_{crit}(i) = \frac{n\pi^2 EI(i)}{L(i)^2} \quad (16)$$

$$\text{if } F(i) < \frac{-F_{crit}(i)}{SF}, \text{ then fail} \quad (17)$$

$$\text{if } F(i) < \frac{-\sigma_{ult,c}(i) A(i)}{SF}, \text{ then fail} \quad (18)$$

$$\text{if } F(i) > \frac{\sigma_{ult,t}^{(i)} A^{(i)}}{SF}, \text{ then fail} \quad (19)$$

Note that standard sign convention for forces is used (compressive forces are negative) and that for each individual member, $\sigma_{ult,c}$ is the ultimate compressive stress, $\sigma_{ult,t}$ is the ultimate tensile stress, EI is the flexural rigidity, and A is the cross sectional area.

Two different values for the buckling end condition factor, n , are considered in this optimization. The first is based on the torsional failure results presented in the torsional strength testing section above. In those tests the failure torque was bracketed as being between 0.24 Nm and 0.255 Nm. Using the lower strength value and an end condition factor of $n = 2.72$ will lead to the analysis predicting the truss being *just* able to withstand the loading, with a very small increment in torque then leading to failure via local shear web buckling – which was exactly the failure mode observed in testing. This value of the end condition factor lies between those for fixed-fixed end conditions ($n = 4$) and fixed-pinned end conditions ($n = 2$). While derived from repeated experimental results, it is not known if this value of end condition factor will hold over the wide range of truss sizes explored here so a second, much more conservative, end condition factor of $n = 1$ will also be considered. This value represents pinned-pinned end conditions, and while the actual bonded end conditions should always be considerably stiffer than pinned joints, using this value sets a conservative lower limit on the buckling strength that can be expected.

Optimization Results

We will now consider the results of this optimization routine for a variety of different conditions. While the analysis methods used are low-fidelity and have not been validated over the wide range of geometries and loadings considered here, the results presented can still be considered to offer an initial idea of the range of performance that may be achievable with wound composite truss structures.

First, consider the optimized Pareto frontier for the wound trusses under a loading factor of $k_p = 1000$, and with the buckling end condition factor equal to the experimentally measured value of $n = 2.72$. In Figure 14a we see that even under this highly loaded condition, the levels of flexural rigidity obtainable by the trusses at a given mass per unit length are significantly higher than those of the commercially available tubes across the entire range of linear densities considered.

We can consider these same results in a manner which makes the differences more clear if we show the ratio of the truss rigidity to that of the tubes. In this instance, only the data for the pull wound tubes is used, as they

outperform the other tubes in this metric. This ratio shows the improvement in EI achievable at a given mass per meter by using trusses instead of tubes, and as seen in Figure 14b the improvement obtainable is considerable. While varying over the linear density range considered, the trusses are between one and two orders of magnitude stiffer than tubes of the same mass, even at this high level of truss loading. This significant increase in stiffness is achievable because the very low linear density obtainable with a given size of truss allows the optimizer to increase the height of the truss with very little mass penalty, which directly takes advantage of the non-linear increase in second moment of area with height.

In order to study the interaction between the geometric parameters of the trusses and their resulting performance against the two objectives, it is useful to consider the parallel coordinates plot shown in Figure 15. In this figure the four different geometric variables are shown alongside the two objectives, and lines representing each individual truss geometry on the Pareto frontier are shown. The geometric variables are normalized by the optimization bounds shown in Table 1, while the objectives are normalized to the range of values seen, with 0 representing the minimum and 1 representing the maximum value present in the Pareto optimal population. The lines are colored according to the flexural rigidity of that individual. It can be seen that the linear density and flexural rigidity are closely correlated. Several of the tube sizes are never selected; likely due to their higher relative wall thickness and corresponding lower structural efficiency. The optimal shear web angles are overall quite tightly grouped, as will be investigated further below. Overall, the trends seen in Figure 15 are reasonable and expected: taller trusses with larger chord members and thicker shear webs have higher flexural rigidity at the expense of higher mass per unit length. Furthermore, the upper and lower bounds chosen for the various geometric parameters are in the end appropriate, as they have not limited the optimization.

We now consider the impact that changing the level of tip loading applied has on the truss structures. Figure 16a shows the Pareto frontiers obtainable by the truss structures under varying amounts of tip load, as governed by the linear density and the loading factor k_p , according to Eq. 15. In Figure 16b the same results are plotted on a log-log scale to better show the trends of the truss results relative to the tubes over the very large range of values obtained. There are several interesting trends in these results. The first is the direct, almost linear, impact that the applied load has on the maximum obtainable EI at a given density. Relaxing the load applied by a factor of one half generally leads to a doubling of the obtainable EI , although there is not necessarily exactly a factor of two increase. This is particularly true for the lower linear densities where there are fewer viable tubing options, which creates a more

stepped shape in the Pareto frontiers. Another interesting trend is that in all cases, the improvement over the tubes in a relative sense can be seen to be higher for the lower linear densities. This reflects the results shown in Figure 14b. This is likely an artifact of the tube sizes shown (which have very thin relative wall thickness at the higher linear densities) and the lack of strength analysis for the tubes. As shown in Figure 13, the relative wall thickness (denoted by the ratio of wall thickness to outer diameter) of the tubes considered decreases significantly with increasing diameter. This indicates that the actual achievable strength in bending as a portion of the ideal strength from a simple cross-sectional analysis is likely to decrease significantly as they scale up in size. As stated previously, a direct strength comparison is outside the scope of this work; a more detailed understanding of this behavior is left to future work. Overall though, it is clear that the truss structures provide significant increases in flexural rigidity for a given density, or alternatively a significant reduction in mass for a given EI requirement, over the entire range of values studied.

As mentioned, one of the primary physical mechanisms by which truss structures increase their efficiency is by taking advantage of height. Indeed, the trusses along the Pareto frontiers in Figure 16 are taller at a given linear density than the tubes against which they are compared. For example, consider that the pullwound tube with a linear density of $\lambda = 100.5$ g/m has an outer diameter of 21 mm, an inner diameter of 19 mm and an EI of 614.1 Nm². The truss which comes closest to matching this linear density (with $\lambda = 100.45$ g/m) is made from three much smaller tubes (5 mm outer diameter and 4 mm inner diameter) and has a total projected vertical height of 186.9 mm and an EI of $27,800$ Nm². For equivalent mass, the truss is able to obtain 8.9 times the height of the tube and over 45 times the flexural rigidity.

For many types of structures this approach to maximizing structural efficiency by increasing the size of the cross section is viable, but there are other applications that may be more restrictive of cross section; for example a wing spar which is constrained to fit within a certain airfoil section. In this case the maximum cross sectional height of the structure will be limited. In instances such as this, it is useful to consider the section modulus S of the truss and tube structures, as this parameter normalizes the second moment of area I by a height dependent parameter y :

$$S = \frac{I}{y} \quad (20)$$

where y is the distance from the neutral axis of the truss/tube to the outermost fiber. For the circular tubes considered, y_{tube} is simply the outer radius, whereas for the equilateral truss cross-sections used here, y_{truss} can be found from the spacing of chord members and the radius of the tubes used for the chord members r_c :

$$y_{truss} = \frac{h/2}{\cos(30^\circ)} + r_c \quad (21)$$

In Figure 17 we see that even after normalizing the results for height, the trusses can still provide an order of magnitude improvement over the composite tubes, especially for the more lightly loaded cases.

Figure 18 shows the effect on the Pareto frontiers of changing the buckling end factor in the strength analysis. If instead of the experimentally measured value of $n = 2.72$ we use the conservative value of $n = 1$ (representative of pinned-pinned boundary conditions), then as expected the flexural rigidity achievable with a given linear density decreases. This reduction in achievable performance is attributable to the reduction in the predicted buckling strength of the shear web. Earlier shear web buckling restricts the truss height obtainable for a given linear density (under a given applied load), thereby affecting the maximum obtainable EI . As the shear web would always be bonded at its ends to the chord members no matter what size of truss the process would be used for, it is likely that the assumption of pinned-pinned boundary conditions is overly conservative. However, even with this limitation the trusses under the highest loading condition ($k_p = 1000$) have at least an order of magnitude higher EI than the tubes and those for the lowest loading condition ($k_p = 125$) have upwards of two orders of magnitude improvement across the entire range of linear densities studied here.

It was noted above that the optimal shear web angles in Figure 15 were tightly grouped. This trend is further illuminated in

Figure 17. Section modulus ($S = I/\gamma$) versus linear density

Figure 18. Effect of buckling end condition factor on Pareto frontiers

Figure 19a, where all of the Pareto optimal individuals for both values of buckling end condition and all four loading levels are overlaid (a total of 16,800 truss geometries). Here we see that the shear web wrapping angles for nearly all of the Pareto optimal individuals fall within the narrow band of roughly $\theta = 37\text{--}41^\circ$, with the average across all the individuals being $\theta = 39.5^\circ$. This is an interesting result as it indicates there is almost a universal shear web angle for maximum efficiency under cantilevered tip loading, which is quite useful from a design perspective.

Another interesting relationship seen in the results is a tight coupling between shear web diameter and length. For the shear web elements of each individual truss, we can define a Slenderness Ratio, SR , as the ratio of effective length to radius of gyration r_g of the shear web. The actual physical length of the shear web member l_{sw} is modified by its buckling end condition factor to give effective length l_{eff} : [25]

$$r_g = \sqrt{\frac{I}{A}} = \frac{d_s}{4} \quad (22)$$

$$SR = \frac{l_{eff}}{r_g} = \frac{l_{sw}\sqrt{1/n}}{r_g} = \frac{h/\cos\theta\sqrt{1/n}}{r_g} = \frac{4h\sqrt{1/n}}{d_s \cos\theta} \quad (23)$$

In

Figure 17. Section modulus ($S = I/y$) versus linear density

Figure 18. Effect of buckling end condition factor on Pareto frontiers

Figure 19b is shown the slenderness ratios of all of the Pareto optimal individuals from all of the optimization cases plotted against flexural rigidity. The slenderness ratios are tightly grouped depending on the applied loading factor, implying a high degree of correlation, and generally speaking there is a gradual increase in the optimal values of SR with increasing EI . The trend of increasing slenderness with decreasing load is understandable in the light of the buckling constraints in the optimization: lower applied loads allow for larger center to center distances (and correspondingly longer shear web member with higher slenderness ratios) before the onset of shear web buckling. This trend is also useful from a design perspective.

While the initial results presented here show that this wound truss technology has the potential to provide significant increases in structural efficiency, it is important to realize that the gains achievable are likely to be more modest in reality, as there are a number of factors which could lead to reduced performance in real world applications. For example, the physical interface between these truss beams and surrounding traditional structural elements, or between multiple truss beams in the case of a space frame will require careful design of fittings and adapters that will invariably introduce additional weight into a real world solution. Other potential concerns include robustness, damage tolerance, and fatigue properties. The strength of the bond between the shear web and the longitudinal members is one area of concern, although local node reinforcement is a useful tool (with an associated cost in complexity of course) should bond strength prove limiting. In general, the failure modes of these structures will need considerable attention in future work, as they will likely also reduce obtainable performance.

This gap between theoretical benefit and real world benefit is of course present in virtually all new material/structural systems, indeed composites generally speaking are only delivering a fraction of their theoretical weight savings in applications such as commercial airliners. However, provided there is large enough of a theoretical benefit to start with, the resulting real world benefit can still bring significant improvement.

Conclusions

In summation, this paper presents the design, analysis, manufacturing, experimental testing, and multiobjective optimization of a new family of ultra-efficient composite truss structures manufactured with a low cost continuous winding process. The continuously wound truss concept is introduced, and a low fidelity analysis method based on a large displacement formulation of the direct stiffness method is presented. Manufacturing and experimental testing of a prototype truss configuration is shown and used to validate the analysis approach. This model is then used to explore the design space achievable with these truss structures through multiobjective optimization using the NSGA II genetic algorithm. Consideration of optimized truss mass, bending rigidity, and load carrying capability shows that these structures can provide between one and two orders of magnitude increase in performance compared to commercially available carbon fiber composite tubes. This work therefore motivates further development of the truss manufacturing technology and refinement of the analysis methods.

Acknowledgements

Portions of this work were funded by the European Research Council under the European Union's Seventh Framework Programme (FP/2007-2013) / ERC Grant Agreement n. [247045].

References

- [1] Klein NL. Evidence for West Greek Influence on Mainland Greek Roof Construction and the Creation of the Truss in the Archaic Period. *Hesperia J Am Sch Class Stud Athens* 1998;67:335–74. doi:10.2307/148449.
- [2] Hodge T. *The Woodwork of Greek Roofs*. Cambridge, UK: Cambridge University Press; 1960.
- [3] Meza LR, Zelhofer AJ, Clarke N, Mateos AJ, Kochmann DM, Greer JR. Resilient 3D hierarchical architected metamaterials. *Proc Natl Acad Sci U S A* 2015;112:11502–7. doi:10.1073/pnas.1509120112.
- [4] Schütze R. Lightweight carbon fibre rods and truss structures. *Mater Des* 1997;18:231–8. doi:10.1016/S0261-3069(97)00056-3.
- [5] Weaver T, Jensen D. Mechanical Characterization of a Graphite/Epoxy IsoTruss. *J Aerosp Eng* 2000;13:23–35. doi:10.1061/(ASCE)0893-1321(2000)13:1(23).
- [6] McCune D. *Manufacturing Quality of Carbon/Epoxy IsoTruss (R) Reinforced Concrete Structures*. MS Thesis. Brigham Young University, 2005.
- [7] Lai C, Wang J, Liu C, Fan H, Xu B, Wu K. A flexible tooling and local consolidation process to manufacture 1D lattice truss composite structure. *Compos Sci Technol* 2015;113:63–70. doi:10.1016/j.compscitech.2015.03.018.
- [8] Sui Q, Fan H, Lai C. Failure analysis of 1D lattice truss composite structure in uniaxial compression. *Compos Sci Technol* 2015;118:207–16. doi:10.1016/j.compscitech.2015.09.003.
- [9] Gurley A, Beale D, Broughton R, Branscomb D. The Design of Optimal Lattice Structures Manufactured by Maypole Braiding. *J Mech Des* 2015;137:101401. doi:10.1115/1.4031122.

- [10] Vasiliev VV, Razin AF. Anisogrid composite lattice structures for spacecraft and aircraft applications. *Compos Struct* 2006;76:182–9. doi:10.1016/j.compstruct.2006.06.025.
- [11] Vasiliev VV, Barynin VA, Razin AF. Anisogrid lattice structures – survey of development and application. *Compos Struct* 2001;54:361–70. doi:10.1016/S0263-8223(01)00111-8.
- [12] George T, Deshpande VS, Wadley HNG. Hybrid carbon fiber composite lattice truss structures. *Compos Part Appl Sci Manuf* 2014;65:135–47. doi:10.1016/j.compositesa.2014.06.011.
- [13] Li W, Sun F, Wang P, Fan H, Fang D. A novel carbon fiber reinforced lattice truss sandwich cylinder: Fabrication and experiments. *Compos Part Appl Sci Manuf* 2016;81:313–22. doi:10.1016/j.compositesa.2015.11.034.
- [14] Dong L, Wadley H. Shear response of carbon fiber composite octet-truss lattice structures. *Compos Part Appl Sci Manuf* 2016;81:182–92. doi:10.1016/j.compositesa.2015.11.015.
- [15] Woods BKS, Berry BO, Stavnychi VB. Continuous wound composite truss structures. US Patent Application No. US20130291709 A1, 2013.
- [16] Berry B, Bowen-Davies G, Gluesenkamp K, Kaler Z, Schmaus J, Staruk W, et al. Design Optimization of Gamera II: a Human Powered Helicopter. *Proc. 68th Am. Helicopter Soc. Annu. Forum*, Fort Worth, TX: 2012.
- [17] Kardestuncer H. Elementary matrix analysis of structures. New York, NY: McGraw-Hill; 1974.
- [18] Dill EH. The Finite Element Method for Mechanics of Solids with ANSYS Applications. Boca Raton, FL: CRC Press; 2011.
- [19] Meek JL. Computer Methods in Structural Analysis. 1st ed. London, UK: Routledge; 1991.
- [20] Meyer R. Handbook of Pultrusion Technology. New York, NY: Chapman and Hall; 1985.
- [21] Shaw-Stewart DE. Pullwinding. *Proc 2nd Int Conf Autom. Compos. PRIBCSUSAF Leeuwenhorst NL*, 1988, p. 26–8.
- [22] Gibson RF. Principles of Composite Material Mechanics, Third Edition. Third Edition. Boca Raton, FL: CRC Press, Taylor and Francis Group; 2012.
- [23] Sims GD, Johnson AF, Hill RD. Mechanical and structural properties of a GRP pultruded section. *Compos Struct* 1987;8:173–87. doi:10.1016/0263-8223(87)90068-7.
- [24] Deb K. Multi-Objective Optimization Using Evolutionary Algorithms. vol. 16. John Wiley & Sons; 2001.
- [25] Donaldson BK. Analysis of Aircraft Structures: An Introduction. Cambridge, UK: Cambridge University Press; 2008.
- [26] Jensen D. Complex composite structures and method and apparatus for fabricating same from continuous fibers. US Patent No. 7,132,027 B2, 2006.

Figure Captions

Figure 1. The incredible scale range of engineered truss structures a). micrometer scale structures created with Two Photon Lithography Direct Laser Writing[3] and b). the Ikitsuki Bridge, the longest continuous span truss bridge in the world at 400m

Figure 2. Schematic of braiding process for IsoTruss® structures.[26]

Figure 3. Schematic representation of wound truss manufacturing process

Figure 4. The Gamera Human Powered Helicopter with blade spars, airframe, and cockpit made from wound truss structures

Figure 5. Truss member notation for direct stiffness method

Figure 6. Convergence of large displacement analysis versus number of loading steps (torsional loading example)

Figure 7. Example outputs of the DSM analysis: a) cantilevered with tip load, b) three point bending loading and c) torsional loading

Figure 8. Manufactured truss structure showing pultruded carbon fiber chord members and wound carbon tow shear web

Figure 9. Experimental three point bending test setup

Figure 10. Torsional stiffness test rig

Figure 11. Experimental validation of direct stiffness method a) three point bending and b) torsional loading

Figure 12. Truss geometry definition for optimization

Figure 13. Details of commercially available tubes used as chord members in the optimization

Figure 14. Comparison between highly loaded wound truss structure ($k_p = 1000$, $n = 2.72$) and commercially available tubes: a) flexural rigidity versus linear density and b) ratio of rigidities

Figure 15. Parallel coordinates plot showing relationship between truss geometry and optimization objectives for members of the Pareto frontier ($k_p = 1000$, $n = 2.72$)

Figure 16. Pareto frontiers of optimized truss designs ($n = 2.72$), a) linear axes, and b) log-log axes

Figure 17. Section modulus ($S = I/y$) versus linear density

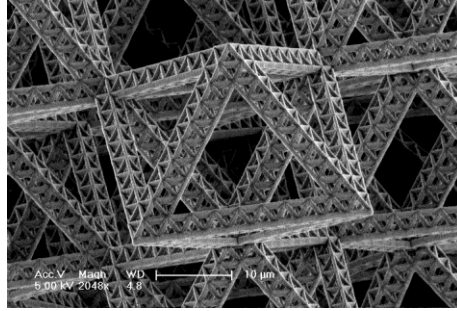
Figure 18. Effect of buckling end condition factor on Pareto frontiers

Figure 19. Optimal shear web angles and shear web slenderness ratios versus flexural rigidity

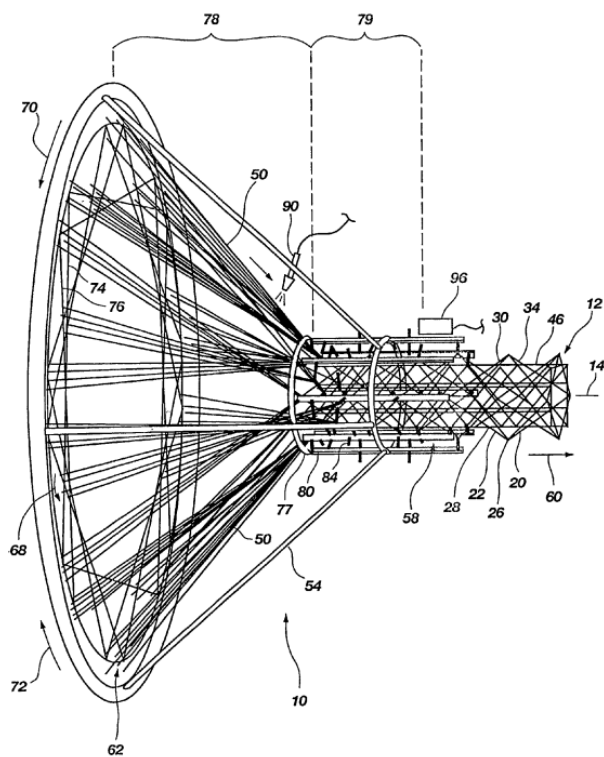
Tables

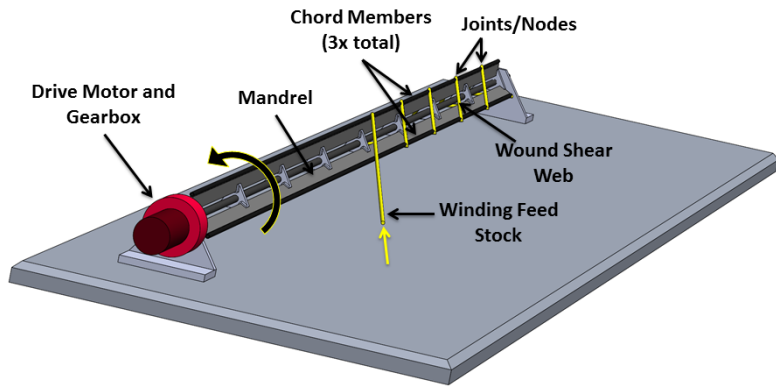
Table 1. Geometry bounds of optimization

Parameter	Variable	Lower Bound	Upper Bound	Units
center-to-center distance	h	0.002	1.5	m
wrap angle	θ	15	80	deg
chord member tube size	n_c	1	34	N/A
shear wrap diameter	d_s	0.4	10	mm



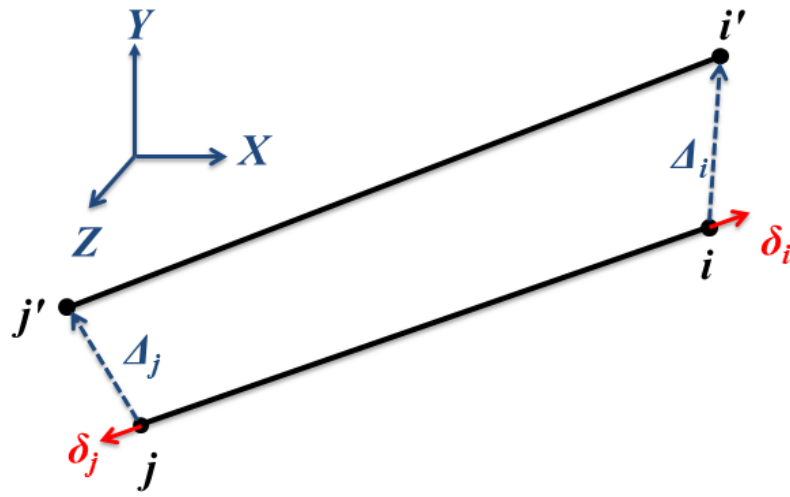
ACCEPTED MANUSCRIPT





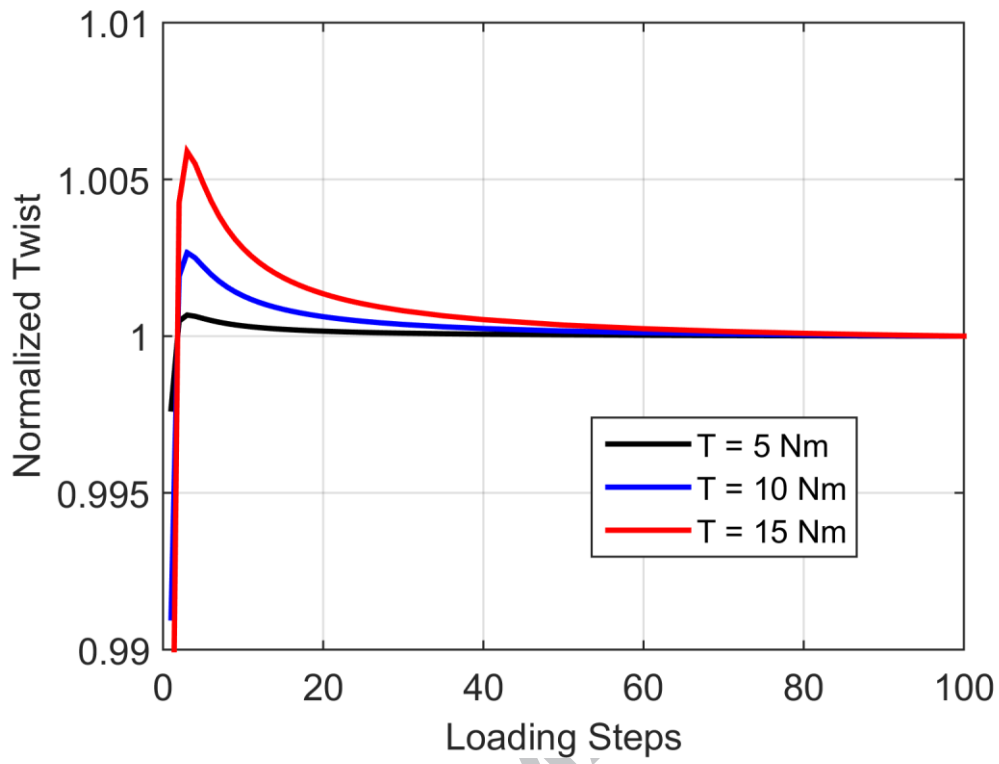
ACCEPTED MANUSCRIPT



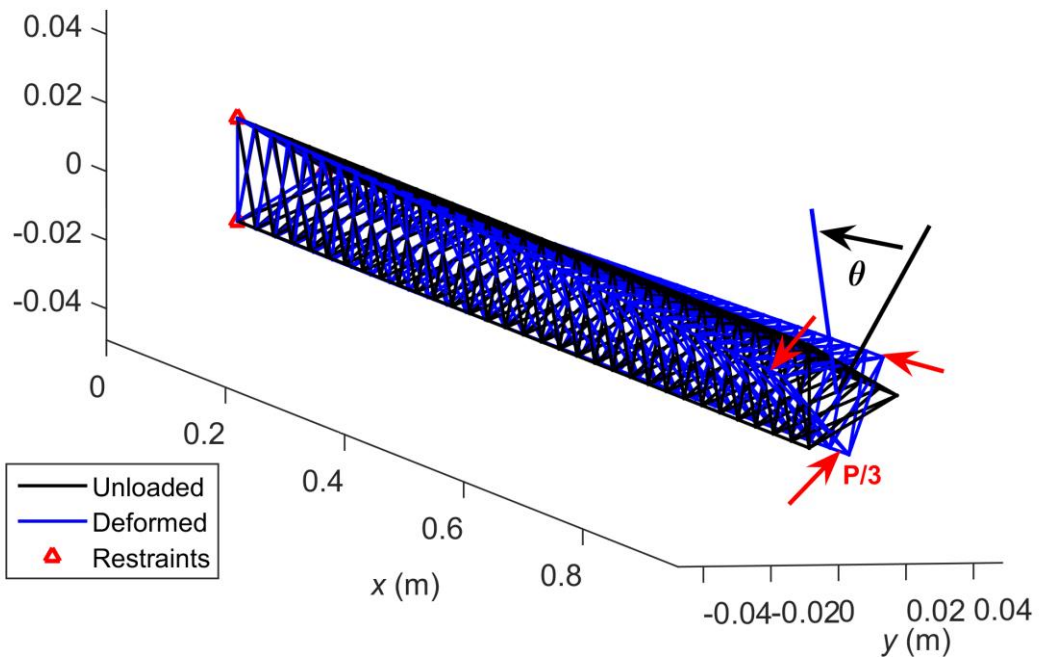
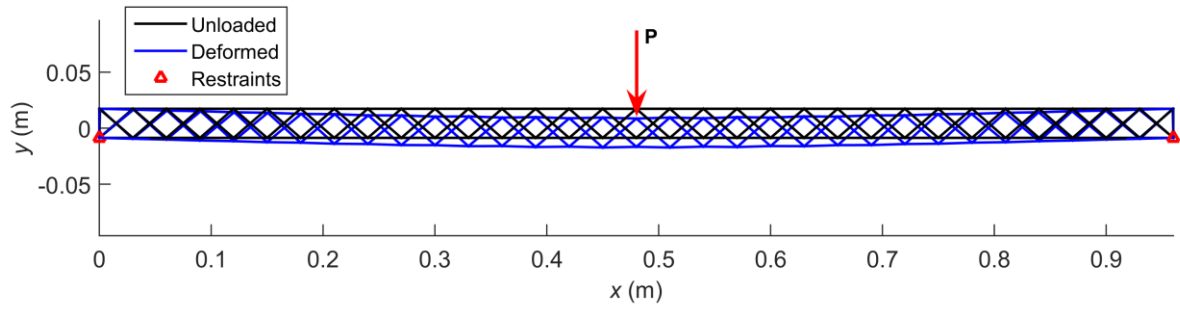
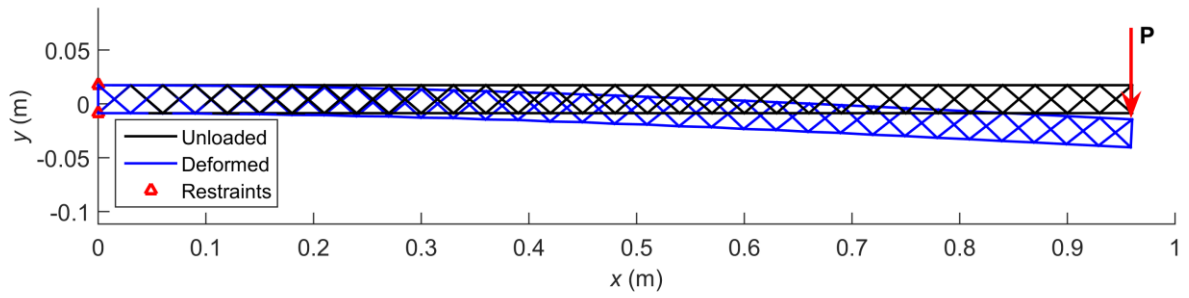


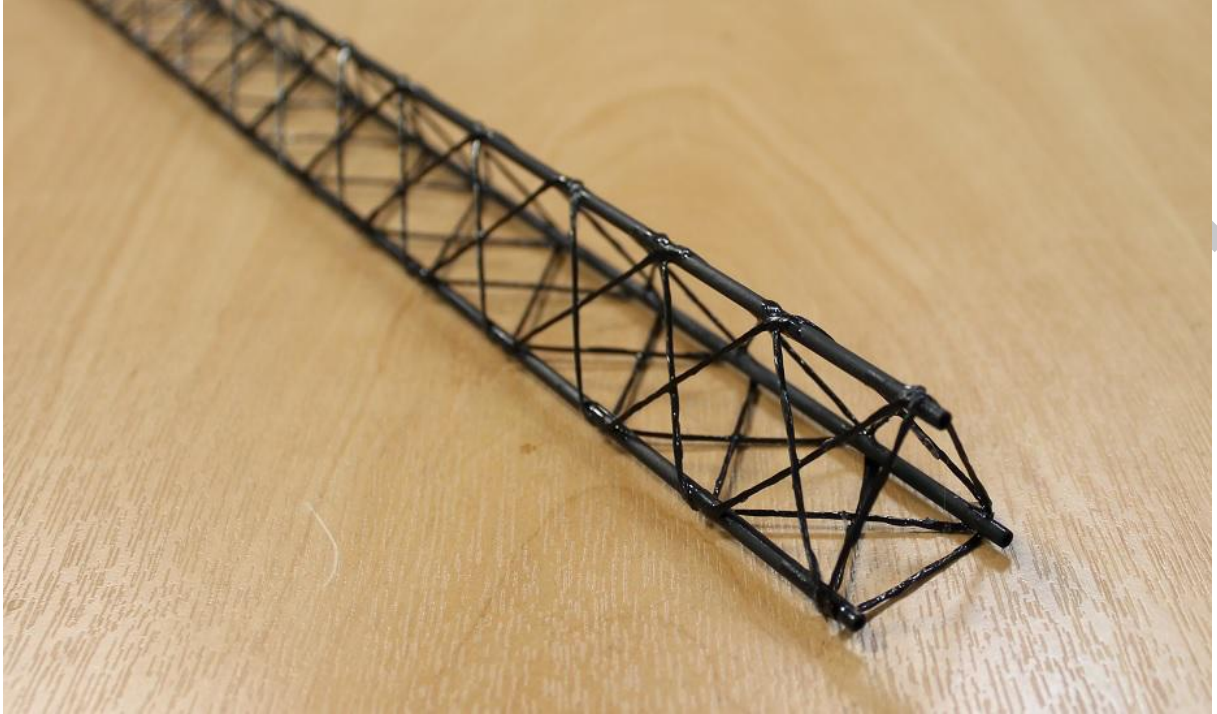
ACCEPTED MANUSCRIPT

IPT

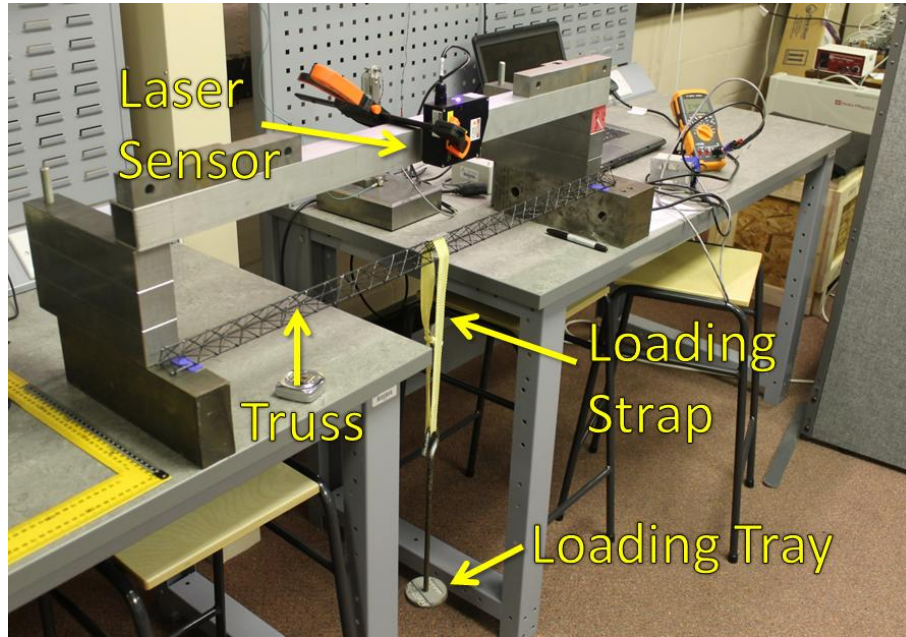


ACCEPTED MANUSCRIPT

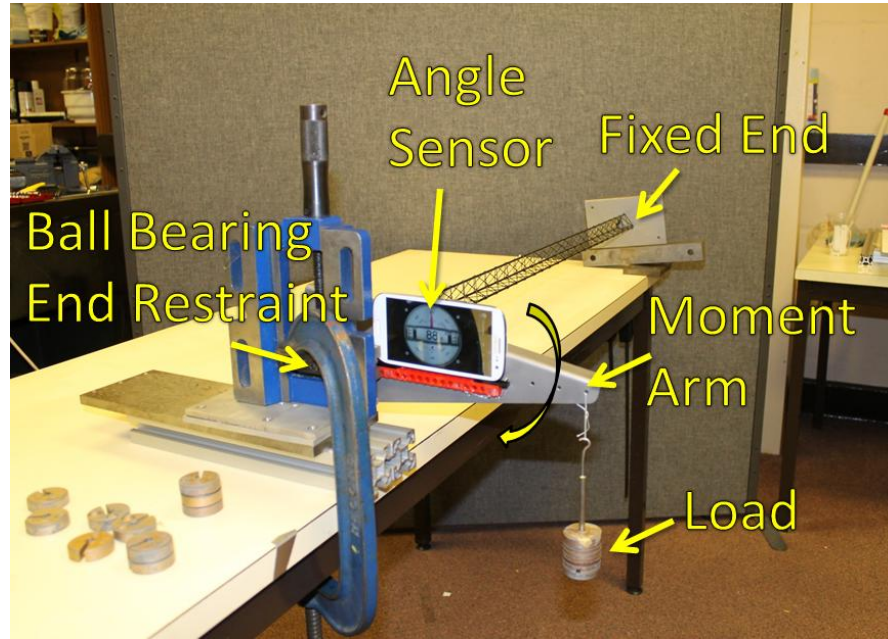




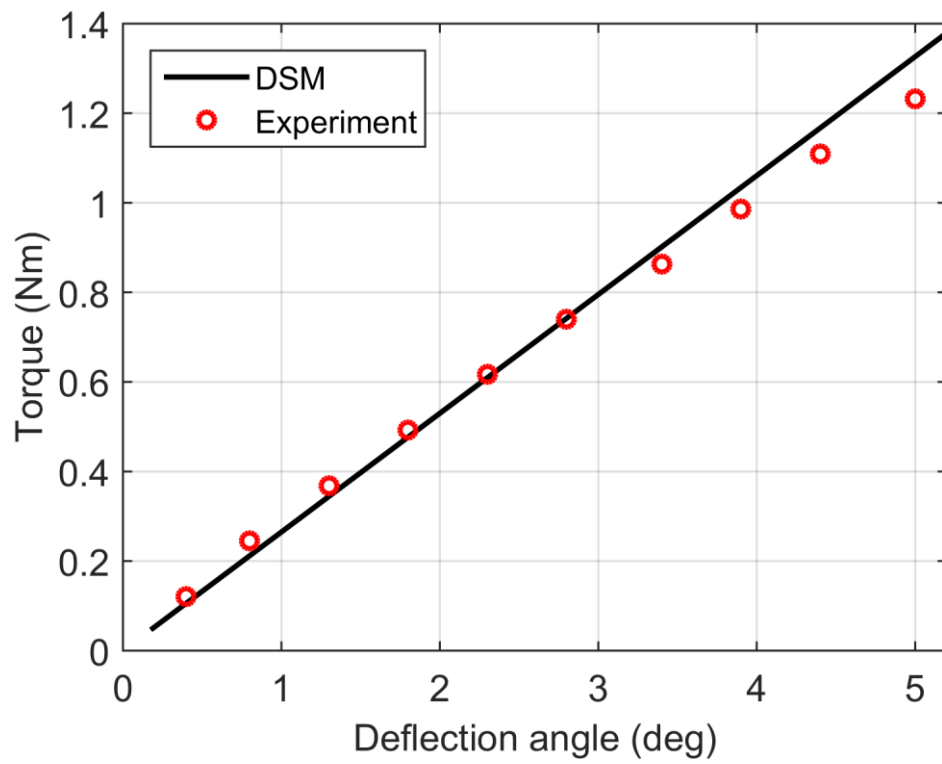
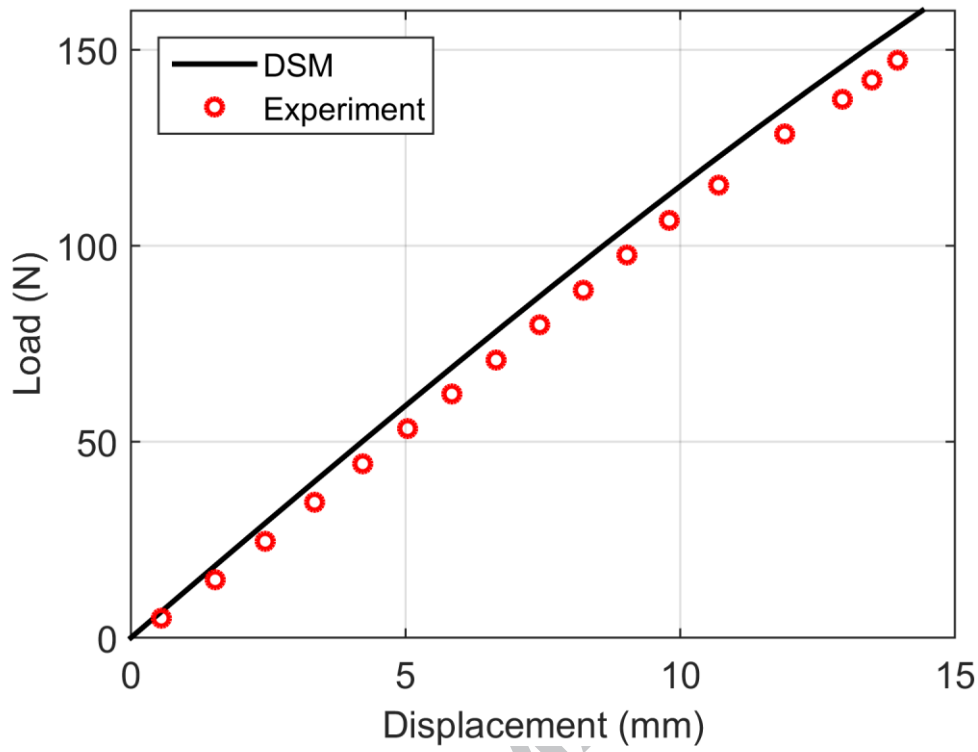
ACCEPTED MANUSCRIPT

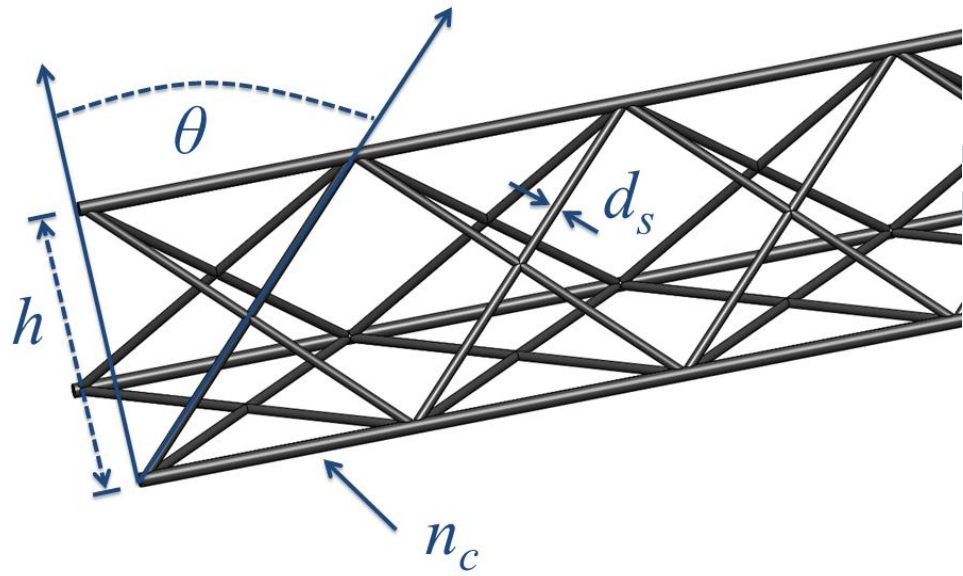


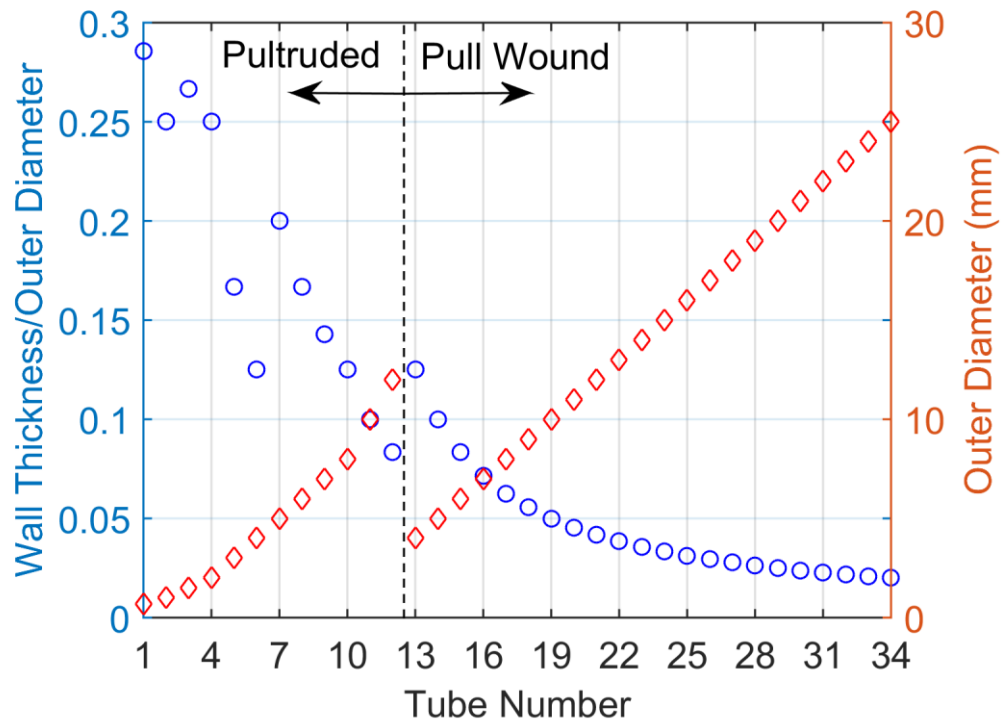
ACCEPTED MANUSCRIPT



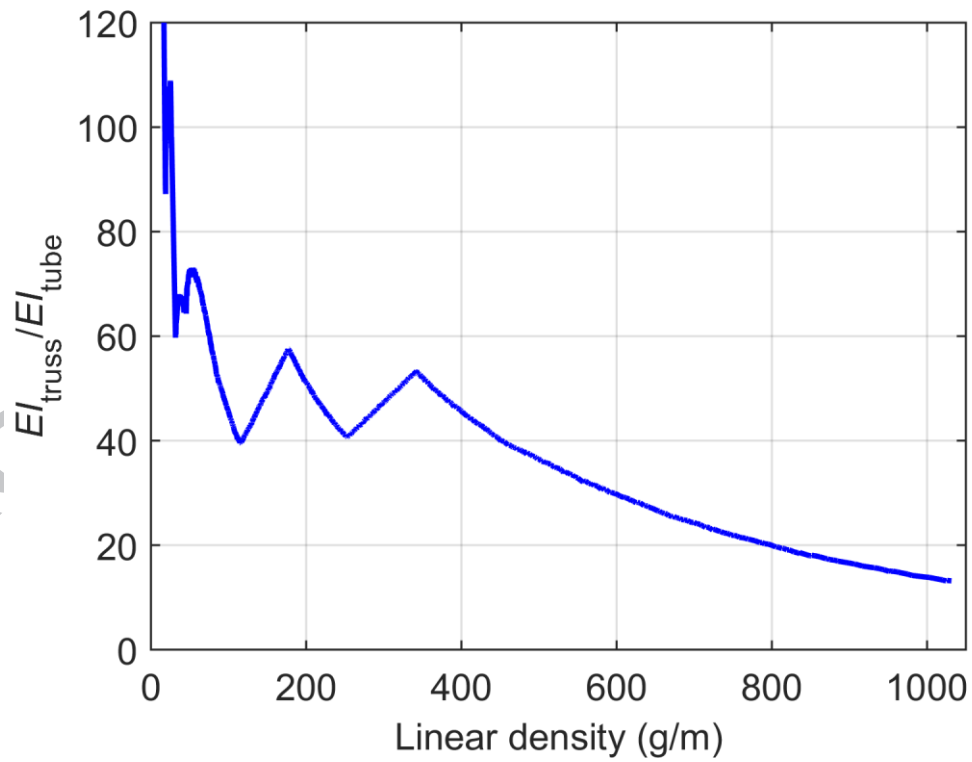
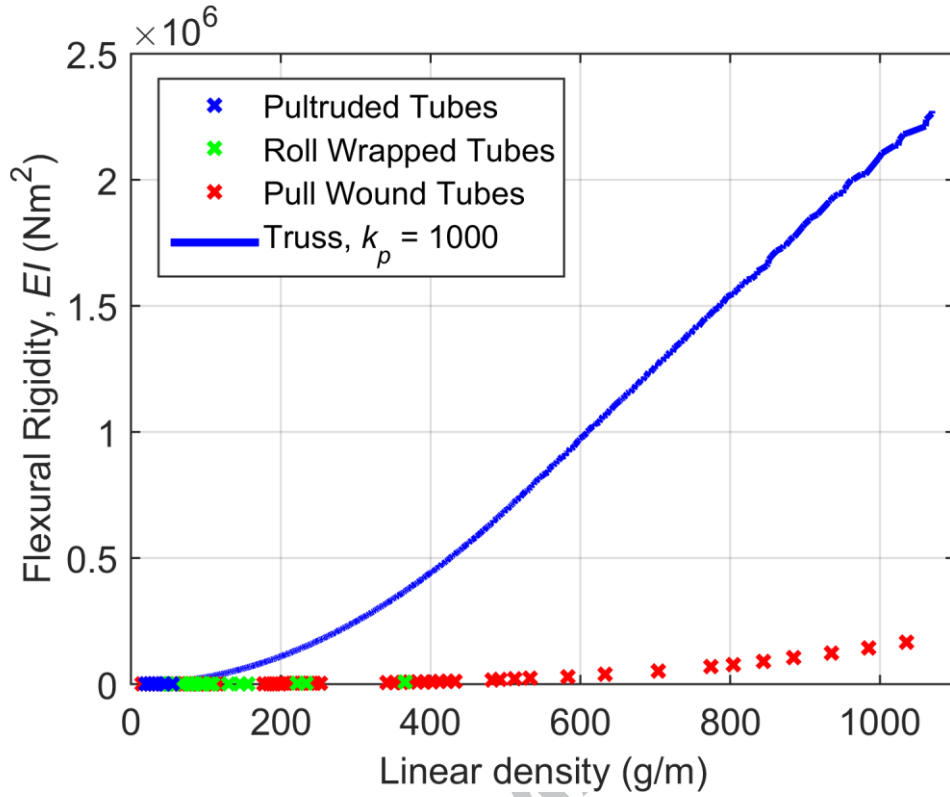
ACCEPTED MANUSCRIPT

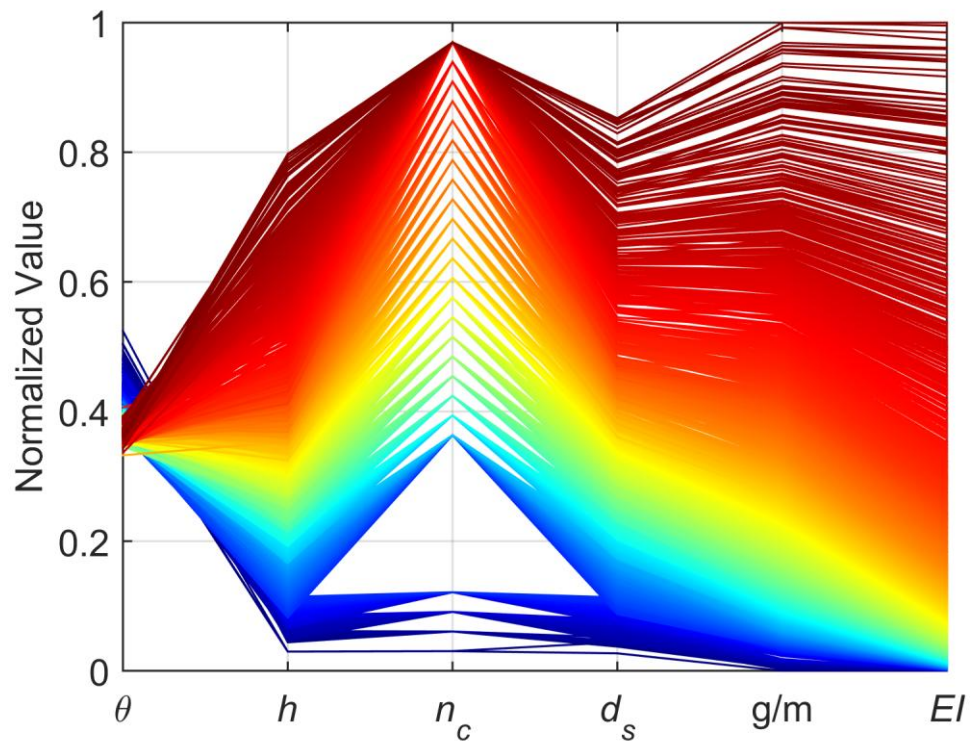






ACCEPTED MANUSCRIPT





ACCEPTED MANUSCRIPT

